An Experimentally Validated Channel Model for Molecular Communication Systems

Na-Rae Kim,* *Member, IEEE*, Nariman Farsad,* *Member, IEEE*,
Andrew W. Eckford, *Senior Member, IEEE*, and Chan-Byoung Chae, *Senior Member, IEEE*

***Abstract*—In this paper, we present an experimentally validated end-to-end channel model for molecular communication systems with metal-oxide sensors. In particular, we focus on the recently developed tabletop molecular communication platform. Unlike previous work, this work separates the system into two parts– the propagation and the sensing. Based on this separation, a more realistic channel model is derived. The coefficients in the derived models are estimated using a large collection of experimental data and it is shown how the coefficients change as a function of different system parameters such as distance, spraying duration, and initial condition. Finally, a noise model is derived for the system to complete an end-to-end system model for the tabletop platform that can be utilized with various system variables. Using this new channel model, we propose a multi-level modulation technique that represents different symbols with different spraying durations while still providing more feasibility and less computational complexity in practice.**

***Index Terms*—Nano communication, molecular communication, channel model, tabletop platform, metal-oxide sensor, experimentation, and experimentally validated models.**

I. Introduction

With the development of nano technology, different kinds of nanoscale machines are being developed such as nano-sensors, nano-motors, or nano switches, and the 2016 Nobel laureates in chemistry were those who developed the world's smallest machines [1]. Along with this trend, networks of these machines are also gaining a lot more interest to create nano networks [2]. The traditional wireless technologies based on radio frequency is one of the options utilizing nano-antennas or nano-transceivers [3], [4]. Another one is molecular communication, inspired from biological systems, that may have several advantages over the traditional wireless technologies due to its scale, energy efficiency, and biocompatibility [5], [6]. Recently it has also been considered as a macroscale communication mechanism in certain scenarios [7], [8].

In molecular communication, information is transferred via chemical signals, or molecules. Unlike traditional wireless communication systems, molecules are used to physically carry information [5]. The transmitter releases molecules, often called messenger/information molecules, that propagate through diffusion [9]–[11], medium flow [12], [13], or active transport [14], [15] to arrive at the receiver side. The channel characteristics and hence the channel models differ depending on the propagation mechanism.

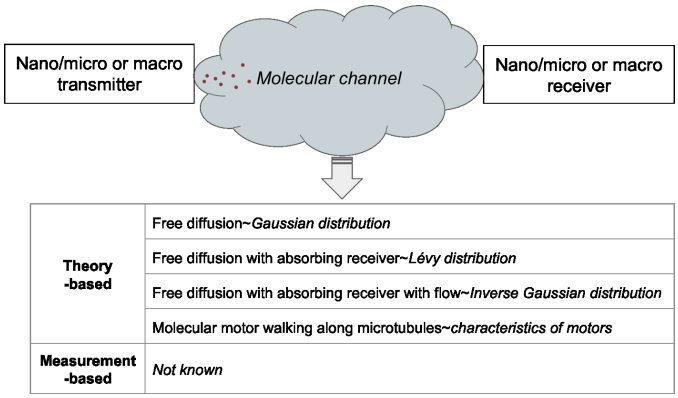

Fig. 1. Theory-based and measurement-based molecular channels.

The information can be encoded in several ways. For example, different information can be represented with different physical/chemical characteristics of the messenger molecules– concentration, number, and/or type [13], [16], [17]. It is also possible to encode messages in the timing-of-release of messenger molecules, which can be considered as pulse position modulation (PPM). There are also advanced techniques that may increase data rate further or decrease inter-symbol interference (ISI) and peak-to-average-molecule ratio (PAMR) [18], [19], In [20], messenger molecules, which are appropriate for medical applications, were suggested [20].

In the literature, most prior work has focused on the communication via diffusion, or flow-assisted diffusion. Most of these works consider only a theoretical analysis of these systems by simplifying assumptions, with no experimental evaluations. The authors in [20] analyzed the achievable data transmission rates of diffusion-based systems, where information is encoded in the type and concentration level of molecular. Other works have focused on the information theoretic capacity analysis of [11], [21]–[23]. Some potential applications have been addressed in [2], and one of the promising applications for molecular communication is considered to be the biomedical field [24], [25].

In this work, we bridge the gap between theory and practice by providing channel models for the first experimental plat-

∗ The authors have equally contributed.

N.-R. Kim is with the Information Systems Technology and Design Pillar, Singapore University of Technology and Design, Singapore. Email: narae_kim@sutd.edu.sg

N. Farsad is with the Department of Electrical Engineering, Stanford University, CA, USA. Email: nfarsad@stanford.edu

A. W. Eckford is with Department of Electrical Engineering and Computer Science, York University, Canada. Email: aeckford@yorku.ca

C.-B. Chae is with the School of Integrated Technology, Yonsei Institute of Convergence Technology, Yonsei University, Korea. Email: cbchae@yonsei.ac.kr

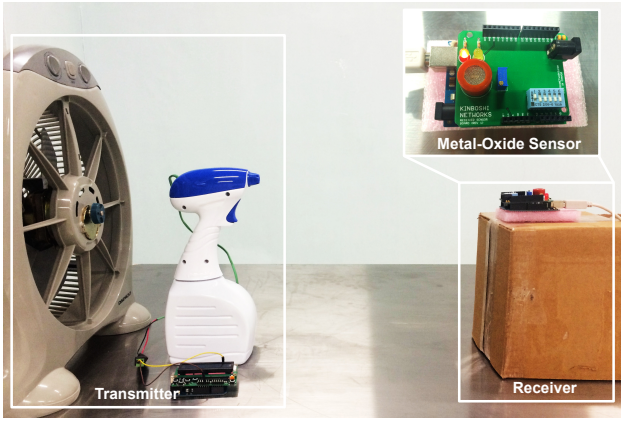

(a) The tabletop platform with the MQ-3 metal-oxide sensor.

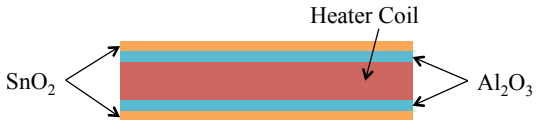

(b) The MQ-3 sensor anatomy.

Fig. 2. The test bed components.

form for molecular communications developed in [26]. This system, which was designed to be inexpensive and flexible, proved the feasibility of molecular communication, especially at macroscales. This testbed has an electronically controllable spray that acts as a transmitter, a metal-oxide gas sensor that acts as a receiver, and a fan to assist the propagation. Two Arduino microcontrollers are also used to control the actions of the transmitter and the receiver. Figure 2 highlights this system and its different components. Later the same system was expanded into a multiple-input multiple-output (MIMO) setup [27].

One of the main advantages of molecular communications is its multi-scale property: molecular communication can be used both on the microscale and macroscale. Although the tabletop platform designed in [26] is a macroscale system, some of the components can be shrunk to micro- and nanoscale. For example, metal-oxide sensors can be easily shrunk to a nanoscale, and be used for detection of different biological compounds [28], [29]. Therefore, understanding how these sensors work can be very beneficial for both macroscale and microscale molecular communication.

As shown in [30], the system response of this testbed departs from the previous theoretical channel models used in the literature. Moreover, it was shown that the system tends to be nonlinear, where the nonlinearity can be successfully modeled as Gaussian noise. In [30], corrections were introduced to the theoretical channel models based on experimental results. However, only a fixed system condition, i.e., a single separation distance between the transmitter and the receiver and a single spray duration, was considered.

In this work, we build on our previous work and derive a more realistic analytical model for the testbed. The new contributions in this work (compared to [30]) are as follows:

- We consider a system model where the sensor and particle propagation are two separate systems. Previous work has modeled the tabletop platform as one system. By using two separate systems connected in series, we achieve a more realistic model.
- We consider the end-to-end system response and how it changes with different system variables such as distance, spraying duration, and initial voltage (i.e., the initial concentration of the messenger molecules in the environment). Our previous work has considered a system model based only on a fixed set of system variables.
- A newly defined additive noise model is also presented for this system, where it is used to capture the randomness of the impulse responses.
- A multi-level modulation technique is considered that can represent different bits of information using multiple spraying durations. In [26], [30], only two levels (i.e., no spray or a spray for a fixed duration) is considered. It is demonstrated that it is possible to use more than two levels while achieving reliable communication. This can be used to increase data rate.

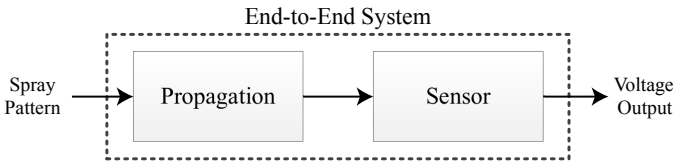

Fig. 3. Block diagram of an end-to-end system.

Since the device in [26], [30] is now a widely-used system for studying molecular communication, the results presented in this paper represent an important contribution to the field, and will help researchers both design experiments, construct improved communication systems, and better understand the features of the system.

The rest of the paper is organized as follows. Section II investigates the sensor characteristics and defines the channel model function with unknown coefficients. Section III analyzes the effect of the system parameters on the channel response. Section IV establishes a universal channel model with the estimated coefficients. Section V suggests a spraying duration-based modulation technique for practical use. Section VI concludes the paper.

II. System Model

As shown in Fig. 2, the transmitter is a spray, and the receiver is a metal-oxide sensor. A fan is used to assist the propagation, and isopropyl alcohol is used to carry information. Presented in Fig. 3 is the end-to-end system block diagram of the tabletop platform. Essentially, the system input is a spray duration, and the system output is the voltage reading at the alcohol sensor. The system has two components: the propagation module, where the sprayed alcohol signal propagates to the sensor, and the sensor module, where the alcohol concentration is estimated from the sensor voltage.

An impulse input is generated through a very short spray (e.g., 100ms). The system response to the impulse input is the impulse response of the system. In our previous work [30],

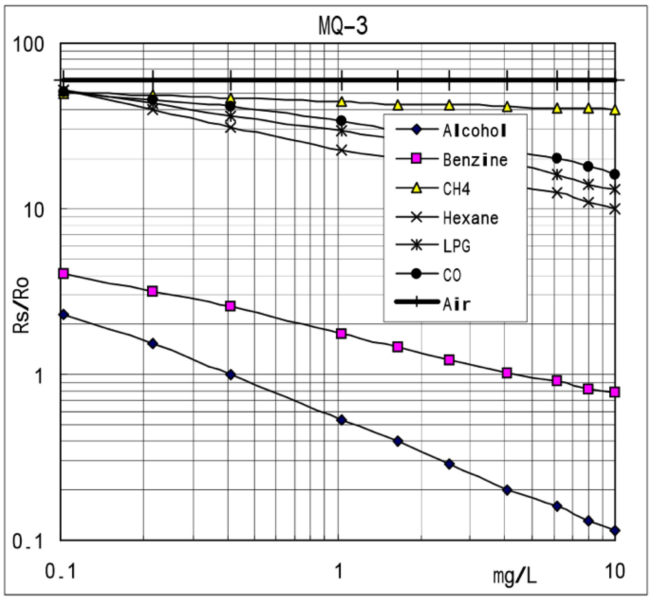

Fig. 4. The sensor sensitivity plot from the datasheet [34].

the end-to-end system response of the system was based only on the chemical propagation model. Specifically, the model considered was

$$C(t) = \frac{a}{\sqrt{t^3}} \exp\left(-b\frac{(d-ct)^2}{t}\right) \tag{1}$$

where a, b, and c are correction factors introduced to match the theoretical and experimental results, and d is the separation distance between the transmitter and the receiver.

In this work, we consider a more accurate model by incorporating the sensor block as well.

A. Metal-Oxide Sensors

The sensor used in the platform is the MQ-3 metal-oxide sensor. Metal-oxide sensors are cheap and can detect various gasses as well as volatile liquids such as alcohol [31]. They can also be shrunk to nanoscale and be used to detect various biological compounds [28], [29]. Moreover, metal-oxide sensors can be used to detect different chemicals [32].

The MQ-3 is a thin-film tin dioxide (SnO_2) sensor, where an aluminium oxide (Al_2O_3) tube is covered with a thin layer of SnO_2. There is a heater coil inside the aluminium oxide made from a nickel-chromium alloy, which is used for resistive heating. Figure 2 shows the anatomy of the MQ-3 sensor.

The sensor works as follows. First, the heater coil heats up the sensing layer (i.e., the SnO_2 layer). According to the sensor's user manual, to achieve the optimal sensor sensitivity, the sensor must be heated 24 to 48 hours prior to use. When the SnO_2 layer heats up, it becomes a semiconductor. When alcohol vapour approaches the sensor, it will go through an oxidization reaction that will in turn change the resistance of the SnO_2 sensing layer [33]. The resistance of the SnO_2 sensing layer decreases as the concentration of alcohol increases in the vicinity of the sensor.

There is a well-known relationship between the resistance of a metal-oxide sensor and the concentration of target molecules [34],

$$R_s \cong a_1 C^n, \tag{2}$$

where R_s is the resistance of the sensor, C is the concentration of molecules, and a_1 and n are constants. In (2), the constant, a_1, is empirically chosen, and the power law exponent, n, is specific to the type of target molecule. This can also be calculated theoretically from the reduced depletion depth and reduced reactivity [34].

To estimate the constant n provided in (2) for the MQ-3 sensor, we use the sensitivity graph in the MQ-3 data sheet. In this graph, shown in Fig. 4, the ratio R_s/R_0 is plotted against the concentration of different target gases. Here R_0 is the resistance of the sensor at a specific concentration of the target gas C_0. In this plot, both axes are in log scale. Therefore, we have

$$\log\left(\frac{R_s(t)}{R_0}\right) \cong \log\left(a_2 C(t)^n\right), \tag{3}$$

where $a_2 = a_1/R_0$ is a new constant. From (3) it is clear that n is the slope of the line corresponding to alcohol in Fig 4. Therefore, we estimate the value of $n = -0.65$, and the sensor resistance is related to the concentration with

$$R_s(t) = a_1 C(t)^{-0.65}, \tag{4}$$

where a_1 is an unknown constant.

B. End-to-End Response

As shown in Fig. 3, the system consists of two stages: propagation and sensor detection. For the propagation phase, the expected system response is given by [35]:

$$C(t) = M\frac{d}{\sqrt{4\pi D t^3}} \exp\left(-\frac{(d-vt)^2}{4Dt}\right), \tag{5}$$

where M is the number of alcohol molecules released by the spray in a short burst; d is the distance between the transmitter and the receiver; D is the effective diffusion coefficient; and v is the average velocity of the wind flow. Substituting (5) into (4), the end-to-end system response is given by

$$R_s(t) = a_1\left[M\frac{d}{\sqrt{4\pi D t^3}} \exp\left(-\frac{(d-vt)^2}{4Dt}\right)\right]^{-0.65}. \tag{6}$$

In [26] and our setup, the change in sensor resistance is measured using a simple voltage divider circuit.

Since it is impractical to measure accurately M, a_1, the effective diffusion coefficient D, and the average velocity v, the end-to-end system response of the system is given by

$$h(t; a, b, c) = a\left[\frac{d}{\sqrt{4\pi b t^3}} \exp\left(-\frac{(d-ct)^2}{4bt}\right)\right]^{-0.65} \tag{7}$$

where a, b, c are unknown coefficients, and d is the distance between the transmitter and the receiver. Specifically, a is the product of constant a_1 and the number of transmitted molecules M; b is the effective diffusion; and c is the average velocity. By obtaining the proper values for the coefficients,

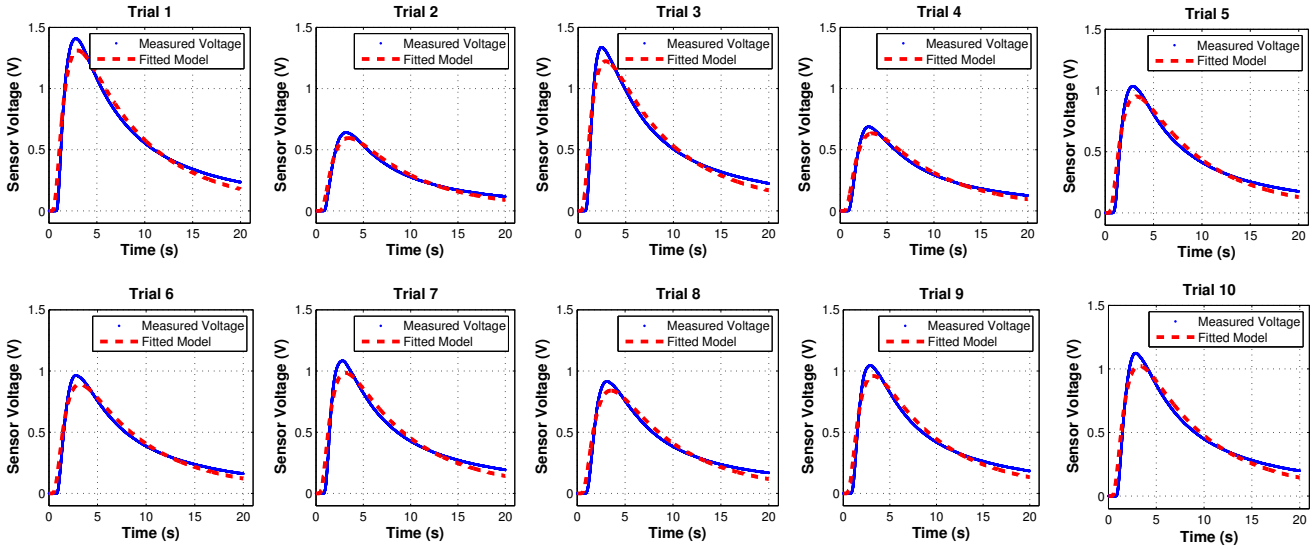

Fig. 5. One fitting example with three unknown coefficients when system parameters are 2 m, 150 ms, and 1.3 V.

TABLE I
SYSTEM PARAMETERS AND DATA SETS PARTITION FOR INTERPOLATION AND EXTRAPOLATION VERIFICATIONS.

Distance (m), d	2	3	4	5
Spraying Duration (ms), s	50	100	150	200
Initial Voltage (V), ν	1.0	1.3	1.6	1.9
Total data sets, $\mathcal{F} = \mathcal{F}(d, s, \nu)$				
	Training data	Testing data		
Model 1 data set	$\mathcal{F} - \mathcal{F}(3, 100, 1.6)$	$\mathcal{F}(3, 100, 1.6)$		
Model 2 data set	$\mathcal{F} - \mathcal{F}(5, 200, 1.9)$	$\mathcal{F}(5, 200, 1.9)$		

a generalized universal model can be established. In the next section, we use experimental data to estimate the values of these three coefficients, and observe how they change with respect to different system parameters.

III. A Channel Model Based on Experiments

To find the value of the unknown coefficients as a function of system parameters, the tabletop platform shown in Fig. 2 is used to measure the end-to-end impulse response of the system using, isopropyl alcohol. To see the effects of different system parameters on the channel responses, the following three system parameters are considered: the *distance* between the transmitter and the receiver, the *spraying duration* (which is related to the number of the transmitted molecules), and the *initial voltage or initial concentration* of the messenger molecules in the environment. Each parameter is varied over four different values as shown in Table I. Therefore, there are 4×4×4=64 different cases, and the end-to-end impulse response of each case is measured across 10 different trials. Thus, to collect all the data to estimate the unknown coefficients, in this paper, we carry out 640 sets of experimental trials in total.

Among 64 different combinations, we use 63 for estimating the coefficients (i.e., 630 training data), and leave one case for testing the obtained model. We do this two times and hence obtain two models (Model 1 and 2) which can be tested on the corresponding test case. For Model 1, we keep the experimental results for the case where *distance* = 3 m, *spraying duration* = 100 ms, *initial voltage* = 1.6 V, and the estimate the coefficients using the remaining 63 cases. For Model 2, the data set where *distance* = 5 m, *spraying duration* = 200 ms, *initial voltage* = 1.9 V is used for testing and the remaining data sets are used for estimating the coefficients.

Here, for Model 1, the testing data set is constructed within the ranges of the known system parameters. Therefore, the process of obtaining Model 1 that fits to this testing data would be interpolation. Similarly, for Model 2, the testing data set is constructed beyond the remaining data set, so it would be extrapolation process to obtain Model 2 that fits to this data. For example, if Model 1 fits to the chosen testing data, we can say interpolation works in this model, and can apply other values within the range such as 2.5 m cases.

A. Coefficients

To estimate the value of the unknown coefficients in the analytical end-to-end model (7), we use a nonlinear least squares curve-fitting technique used in our previous work [30]. Assuming that there are N points in the sensor measurement from each trial, then (7) can be discretized as $h(t_k, \mathbf{p})$ ($k \in \{1, 2, \cdots, N\}$), where t_k are sampling times, and $\mathbf{p} = [a, b, c]^T$ is the parameter vector representing the three unknown constants. The coefficient estimation problem can be formulated as

$$\arg\min_{\mathbf{p}} \sum_{k=1}^{N} \big(O(t_k) - h(t_k, \mathbf{p})\big)^2, \tag{8}$$

where $O(t_k)$ represents the experimental observations.

Channel responses for each case are averaged over 10 trials, and the coefficients are estimated using the least squares estimation technique. For example, the fitted results are shown

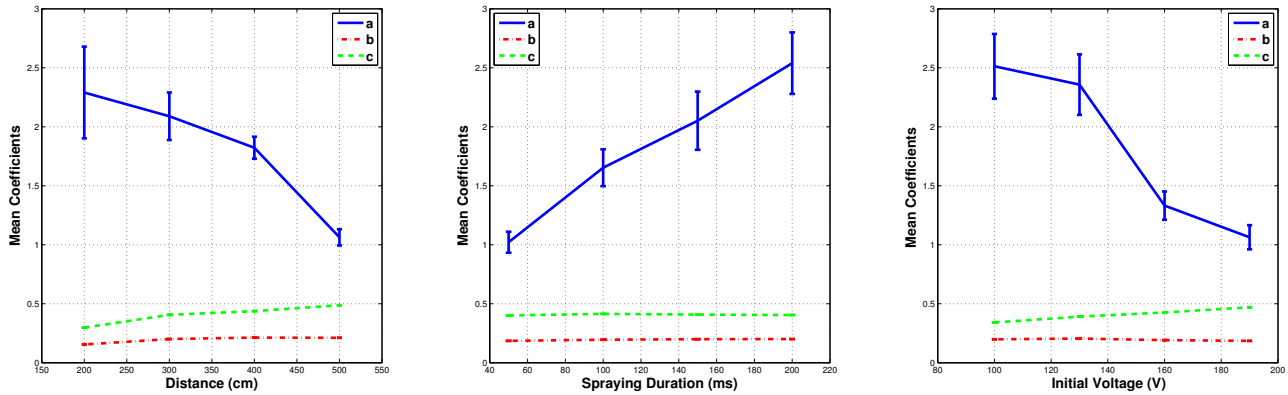

(a) Distance effect. (b) Spraying duration effect. (c) Initial voltage effect.

Fig. 6. The averaged effects of the system variables on the coefficients with Model 1 data set.

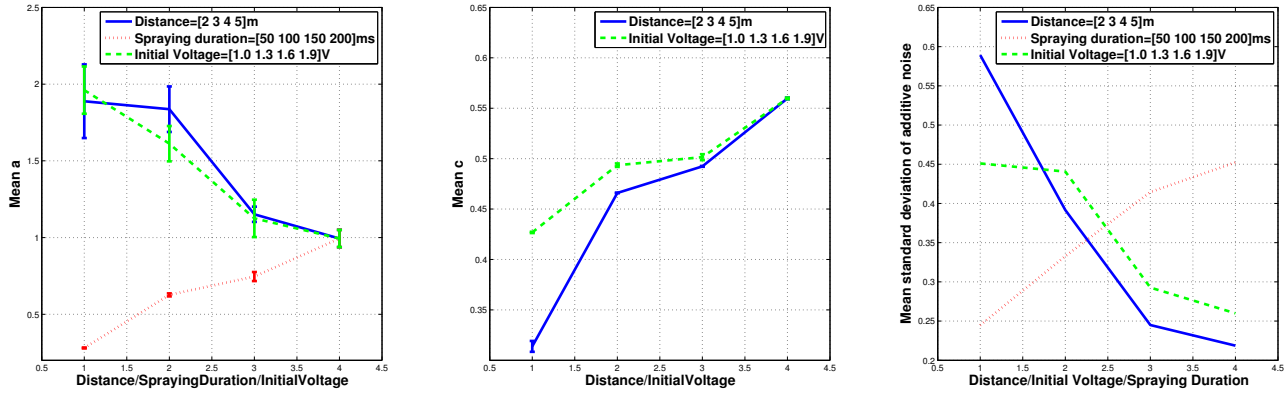

(a) Coefficient a with fixed b. (b) Coefficient c with fixed b. (c) Standard deviation of the additive noise, σ_a, with fixed b.

Fig. 7. The averaged effects of the system variables with fixed b on a, c, and σ_a with Model 1 data set. The x-axis indicates the index of the system variable vectors as shown in the legend.

in Fig. 5 for the case when the distance between the transmitter and the receiver is 2 m, the spray duration is 150 ms, and the initial voltage is 1.3 V. It is apparent that our model function fits very well to the measurement data. The root mean square error (RMSE) with Model 1 is 0.0299, and is 0.0282 with Model 2, which is smaller than with the previous model in [30]. Here, the fitting results are shown only from Model 1 data set to avoid redundancy.

Figure 6 shows the effect of the system parameters on the coefficients. Each point in the plot represents the average value of the corresponding coefficient across 160 trials. The standard-deviation bars represent the standard deviation across trials. As can be seen, coefficient a changes frequently with changing system parameters, while coefficient c varies slightly with respect to system parameters, and b is mostly a constant. Specifically, coefficient a changes with distance, spray duration, and initial voltage; c changes only with distance and initial voltage (i.e., not with spraying duration). These results agree with the physical characteristics of the system. For example, the effective diffusion coefficient is expected to be a constant. From Fig. 6(b), we can see that as the spray duration increases, a increases linearly and the variance of a also increases. This is because more molecules are released as the spray duration increases thereby increasing M in (6). Based on these observations, we assume b to be constant and to be equal to the average values of b over 630 trials. Note that since the variance of b is so small, this is a very good estimation for this coefficient. Let b^* be this average value with $b^* = 0.1950$.

When we perform least squares curve fitting with the fixed coefficient b^* and unknown coefficients a and c, the fitted curves are as good as the ones shown in Fig. 5. Therefore, to avoid duplications, we leave out those plots. Fig. 7(a) and 7(b) show the behavior of the coefficients with the fixed b^*. As can be seen, both a and c change with respect to the system parameters. Let d, s, and ν be, respectively, the distance, spraying duration, and the initial voltage. Then from (7) we have the final end-to-end model as shown in (9).

B. Noise

An important part of the system is the random nature of the end-to-end impulse response. Some of the factors that

$$h(t;a,b^*,c) = a\left[\frac{d}{\sqrt{4\pi b^* t^3}}\exp\Big(-\frac{(d-ct)^2}{4b^*t}\Big)\right]^{-0.65}, a = f(d,s,\nu),\ c = g(d,\nu),$$
$$h(t;d,s,\nu) = f(d,s,\nu)\left[\frac{d}{\sqrt{4\pi b^* t^3}}\exp\Big(-\frac{(d-g(d,\nu)t)^2}{4b^*t}\Big)\right]^{-0.65}, \tag{9}$$

where $h(t;d,s,\nu)$ is a function of time, t, with three coefficients.

TABLE II
THE ESTIMATED β COEFFICIENTS OF MODEL 1.

Coefficient	Value	Coefficient	Value	Coefficient	Value
$\beta_d^{(f)}$	-0.4166	$\beta_d^{(g)}$	0.0708	$\beta_d^{(L)}$	-0.1249
$\beta_s^{(f)}$	0.0099	-	-	$\beta_s^{(L)}$	0.0014
$\beta_\nu^{(f)}$	-1.7799	$\beta_\nu^{(g)}$	0.1358	$\beta_\nu^{(L)}$	-0.2373
$\beta_0^{(f)}$	4.6282	$\beta_0^{(g)}$	-0.0420	$\beta_0^{(L)}$	0.9662

TABLE III
THE ESTIMATED β COEFFICIENTS OF MODEL 2.

Coefficient	Value	Coefficient	Value	Coefficient	Value
$\beta_d^{(f)}$	-0.4162	$\beta_d^{(g)}$	0.0711	$\beta_d^{(L)}$	-0.1272
$\beta_s^{(f)}$	0.0099	-	-	$\beta_s^{(L)}$	0.0014
$\beta_\nu^{(f)}$	-1.7785	$\beta_\nu^{(g)}$	0.1369	$\beta_\nu^{(L)}$	-0.2450
$\beta_0^{(f)}$	4.6204	$\beta_0^{(g)}$	-0.0443	$\beta_0^{(L)}$	0.9878

contribute to the randomness are the spray, which is not precise enough to spray the same amount of alcohol across trials, the random propagation due to diffusion and turbulent flows, and other phenomena such as temperature variations. Therefore, to obtain a complete system model, the random effect must be represented as noise. To establish a noise model, an additive noise is defined as the difference between the experimental observation and the model function shown below.

$$N_i(t) = O_i(t) - h(t;d,s,\nu), \tag{10}$$

where, $N_i(t)$ is the additive noise, and $O_i(t)$ is the observation or measurement for each trial i ($i = 1, 2,\ 10$ for a specific distance, spray duration, and initial voltage). From Figs. 7(a) and 7(b), we can see that for coefficient c, the standard deviation across the trials is small. Therefore, since only coefficient a has a large variance across different trials we have

$$O_i(t) = (f(d,s,\nu)+N)\left[\frac{d}{\sqrt{4\pi b^* t^3}}\exp\Big(-\frac{(d-g(d,\nu)t)^2}{4b^*t}\Big)\right]^{-0.65}, \tag{11}$$

where N is the noise introduced by the system, with

$$N_i(t) = N\left[\frac{d}{\sqrt{4\pi b^* t^3}}\exp\Big(-\frac{(d-g(d,\nu)t)^2}{4b^*t}\Big)\right]^{-0.65}. \tag{12}$$

Let a_{O_i} be the best least squares fit for coefficient a for a trial corresponding to the experimental observation $O_i(t)$. Then a noise sample for N is obtained by:

$$N = a_{O_i} - f(d,s,\nu). \tag{13}$$

Since $f(d,s,\nu)$ is obtained from the average value of coefficient a over different trials, the mean of N becomes zero for all cases. As represented in Fig. 7(c), however, the standard deviation of N changes with system parameters showing behavior similar to a. Thus, it is also possible to express the standard deviation as a function of the system parameters as in analyzing coefficient a.

$$E[N] = 0$$
$$\sqrt{Var[N]} = \sigma_a = L(d,s,\nu) \tag{14}$$

where, $E[\cdot]$ and $Var[\cdot]$ denotes the expectation value and variance, respectively.

IV. A COMPLETE END-TO-END MODEL

In this section, we derive a complete end-to-end model for the tabletop platform. From Section III, coefficient a– the standard deviation of its additive noise, and coefficient c have a close relationship with the system parameters. Therefore, our goal is to estimate a, c, and σ_a as the functions $f(d,s,\nu)$, $g(d,\nu)$, and $L(d,s,\nu)$.

A. Estimating the Coefficient Functions

From Figs. 7(a), 7(b), and 7(c), it can be seen that the coefficients a, c and the standard deviation of the additive noise change relatively linearly with respect to the different system parameters. Therefore we estimate the functions $f(d,s,\nu)$, $g(d,\nu)$, and $L(d,s,\nu)$ as linear functions as shown below

$$f(d,s,\nu) = \beta_d^{(f)}d + \beta_s^{(f)}s + \beta_\nu^{(f)}\nu + \beta_0^{(f)}, \tag{15}$$
$$g(d,\nu) = \beta_d^{(g)}d + \beta_\nu^{(g)}\nu + \beta_0^{(g)}, \tag{16}$$
$$L(d,s,\nu) = \beta_d^{(L)}d + \beta_s^{(L)}s + \beta_\nu^{(L)}\nu + \beta_0^{(L)}, \tag{17}$$

where all the β variables are constants. To estimate the values of the β constants, we use again the linear least squares method. With interpolation and extrapolation data, Tables II and III show the estimated values of these constants.

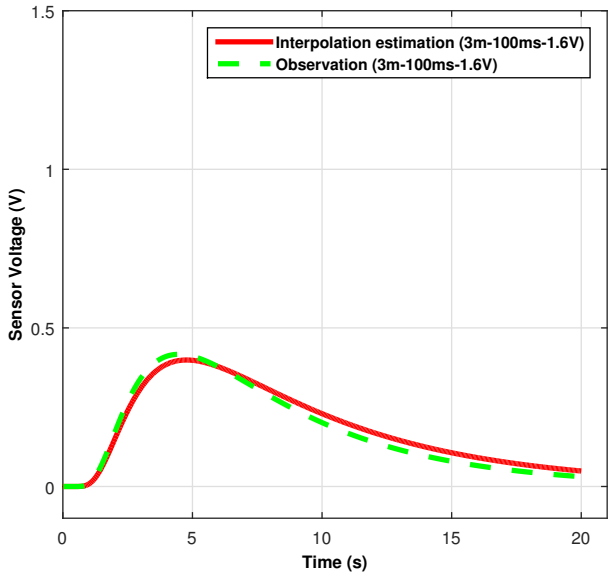

Fig. 8. Comparison of the interpolation estimation from the obtained model and the experimental channel observations.

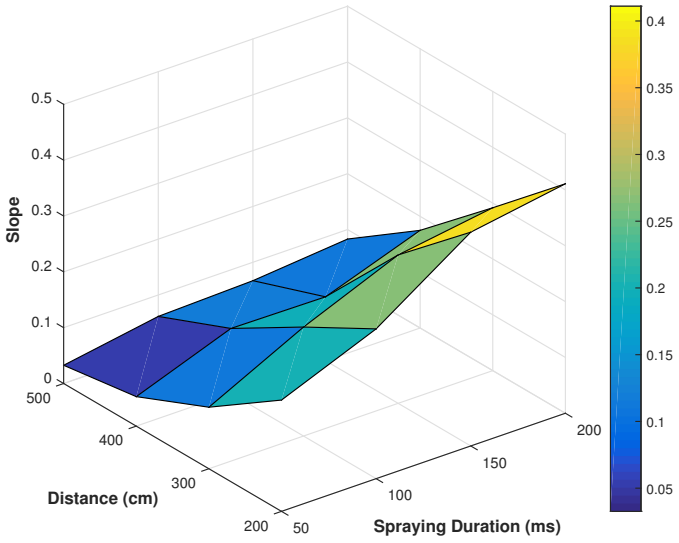

Fig. 9. Average slope of channel responses with different spraying duration and distance.

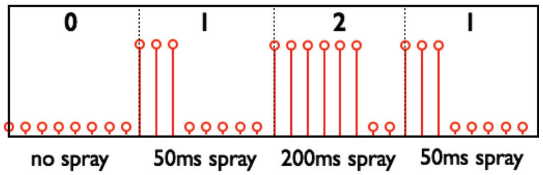

Fig. 10. Conceptual figure of the modulation technique.

B. Verifications

To verify the estimation of the channel coefficients, two testing data sets are selected, as described in Table I. First, the training data sets are used for regression to estimate Models 1 and 2, and the testing data sets are used for verification. Figure 8 describes the comparison between Model 1 and the averaged observations of the Model 1 testing data. It shows that the two results match fairly well, and similar result is also shown in verification of Model 2 (not shown here to avoid redundancy). Thus, it is proved that the newly developed end-to-end molecular channel model can be utilized for various values of the distance, spraying duration, and initial voltage.

V. Modulation Techniques for Practical Use

A great deal of literature is devoted to investigating modulation techniques for diffusion-based molecular communication systems. For example, the various physical or chemical characteristics of the molecules such as concentration level, concentration frequency, type, or ratio can be used to represent different symbols [36], [37]. Timing information is also frequently used by applying different pulse positions, which could easily be combined with other modulation techniques [38]. Such techniques, however, have been analyzed only theoretically, and not considered in a practical setting. Therefore, we can propose based on the measurement data, a more improved version of previous modulation technique that can give more feasibility in practice with less computational and operational complexity maintaining reliable communication.

Recall the completed channel model from Section IV:

$$h(t;d,s,\nu) = f(d,s,\nu)\Big[\frac{d}{\sqrt{4\pi b^* t^3}}\exp\Big(-\frac{(d-g(d,\nu)t)^2}{4b^* t}\Big)\Big]^{-0.65}.$$

There can be several curve features using the model such as peak position (t_{peak}), peak value ($h(t_{\text{peak}})$), delay to start (t_{delay}), and slope of channel responses, which can be utilized to differentiate different channel responses on the receiver side. Here, the moment when the peak occurs in a channel model is referred to as the peak position, and peak value is the maximum value of a channel response. Delay-to-start is the moment when the response starts to change suddenly, and slope is obtained from the peak value divided by the difference between the peak position and the delay-to-start as obtained below.

$$\begin{aligned}&\frac{dh}{dt} = 0 \Rightarrow t_{\text{peak}} = \frac{-6b^* + \sqrt{36b^* + 4d^2 g(d,\nu)^2}}{2g(d,\nu)^2},\\ &\text{peak value} = h(t_{\text{peak}}),\\ &\text{slope} = \frac{h(t_{\text{peak}})}{t_{\text{peak}} - t_{\text{delay}}}.\end{aligned} \tag{18}$$

By performing curve feature analysis, we can formulate several curve differentiation methods. Specifically, slope and peak value change significantly with spraying duration, and Fig. 9 shows the slope behaviour as an example. This can motivate the idea of a multi-level modulation technique that can represent different symbols using different spraying duration. Compared to previously-used modulation techniques [26], [30], duration-based modulation can be easily differentiated using slope or peak values. It is similar to the concentration-

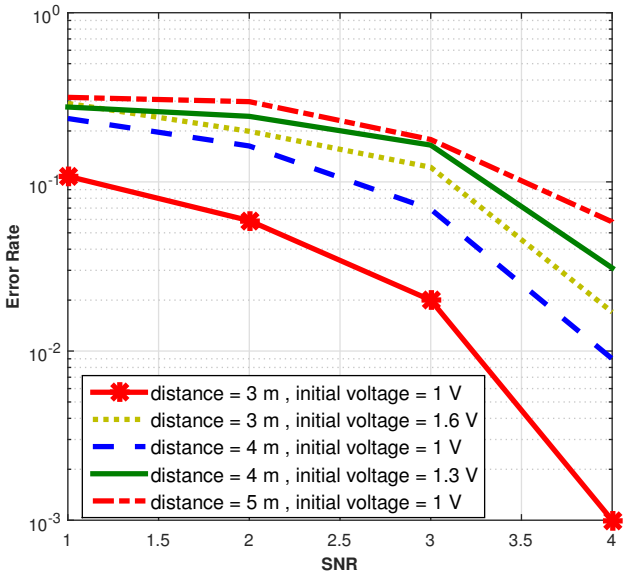

Fig. 11. Error rate comparisons of the used modulation technique.

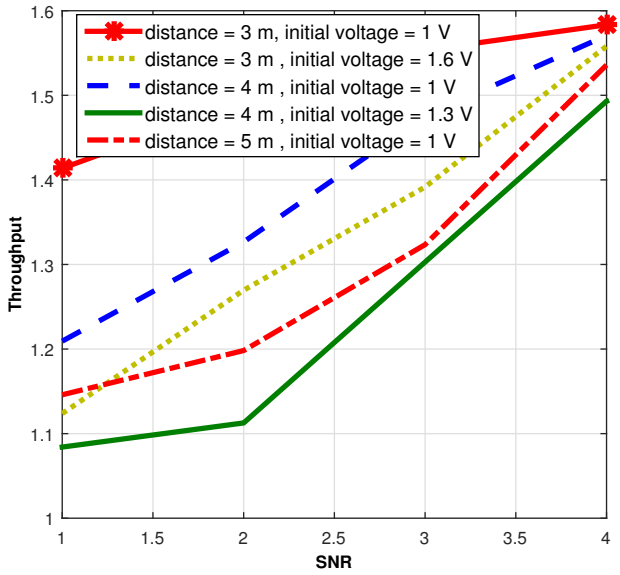

Fig. 12. Throughput comparisons of the used modulation technique.

shift keying (CSK) technique [36], but can be considered as a combination of the square-based and the impulse-based CSK. Therefore, in terms of peak-to-average-molecule ratio or PAMR, it overcomes the high PAMR weakness of the widely-used impulse-based CSK technique [39].

Also, on the practical side, this techniques does not require different types, as in molecule shift keying (MoSK); or different concentrations of messenger molecules, both of which give lower operational complexity. Specifically, a transmitter has to be equipped with multiple reservoirs for different concentrations or different types of messenger molecules to apply CSK or MoSK techniques. On the other hand, spraying duration can be easily controlled in the testbed by the micro-controller that gives lower transmitter complexity. At the receiver side, it may not be easy to recognize the concentration of received molecules with a limited number of receptors, but can be relatively easy to calculate the slope or peak value of the received channel responses as shown in (18).

For example, symbols 0, 1, and 2 can be represented by no spray, 50 ms of spray, and 200 ms of spray, as described in the conceptual figure of Fig. 10. For numerical analysis, Figures. 11 and 12 show the relative comparisons of error rate and throughput with the selected distance and initial voltage cases. It can be seen that the error rate increases with distance and initial voltage, and throughput decreases accordingly as expected. Therefore, we conclude that the used multi-level modulation technique works well providing reliable communication. For future work, it can be deployed with more levels, and further demonstrated using the test bed.

VI. Conclusions

This work proposed an experimentally validated channel model for molecular communication systems with metal-oxide sensors as a function of various system parameters such as distance, spraying duration, and initial voltage. The propagation and the sensing models were considered as separate systems. We collected experimental data for various system parameters. In particular, data was collected for four different distances, four different spray duration, and four different initial voltage, which resulted in 64 different scenarios. Using this data an end-to-end model for the system is developed. An additive noise model was added to the system, and it was shown that these models can represent the system very well. We then considered a multi-level modulation technique that used different spraying durations to represent different symbols. We showed that it is possible to use more levels compared to prior work, while maintaining reliable communication, which increases information rate. Finally, the experimentally validated channel model derived in this work provides a more realistic framework for many researchers studying molecular communication.

Acknowledgement

This research was supported by Basic Science Research Program through the National Research Foundation of Korea (NRF) funded by the Ministry of Education (2016R1A6A3A03006413).

References

[1] Nobelprize.org, "The 2016 nobel prize in chemistry - press release," Oct 5th 2016.

[2] I. F. Akyildiz, F. Brunetti, and C. Blazquez, "Nanonetworks: A new communication paradigm," *Elsevier Comput. Netw.*, vol. 52, no. 12, pp. 2260–2279, Aug. 2008.

[3] J. M. Jornet, , and I. F. Akyildiz, "Channel modeling and capacity analysis for electromagnetic wireless nanonetworks in the terahertz band," *IEEE Trans. Wireless Commun.*, vol. 10, no. 10, pp. 3211–3221, Oct. 2011.

[4] P. Boronina, V. Petrov, D. Moltchanov, Y. Koucheryavya, and J. M. Jornet, "Capacity and throughput analysis of nanoscale machine communication through transparency windows in the terahertz band," *Elsevier Nano Commun. Netw.*, vol. 5, no. 3, pp. 72–82, Sept. 2014.

[5] T. Nakano, A. W. Eckford, and T. Haraguchi, *Molecular communication*, Cambridge University Press, first edition, 2013.

[6] S. Hiyama, Y. Moritani, T. Suda, R. Egashira, A. Enomoto, M. Moore, and T. Nakano, "Molecular communication," in *Proc. NSTI Nanotechnol. Conf. (NanoTech)*, 2005, pp. 391–394.

[7] S. Qiu, W. Guo, S. Wang, N. Farsad, and A. Eckford, "A molecular communication link for monitoring in confined environments," in *Proc. IEEE Int. Conf. on Commun. (ICC)*, 2014.

[8] W. Guo, C. Mias, N. Farsad, and J.-L. Wu, "Molecular versus electromagnetic wave propagation loss in macro-scale environments," *IEEE Trans. Mol. Biol. Multi-Scale Commun.*, vol. 1, no. 1, pp. 1887–1919, Mar. 2015.

[9] T. Nakano, T. Suda, T. Koujin, T. Haraguchi, and Y. Hiraoka, "Molecular communication through gap junction channels," in *Trans. Comput. Syst. Biol. X*, vol. 5410 of *Springer Lect. Notes Comput. Sci.*, pp. 81–99. 2008.

[10] M. Pierobon and I. F. Akyildiz, "A physical end-to-end model for molecular communication in nanonetworks," *IEEE J. Sel. Areas Commun.*, vol. 28, no. 4, pp. 602–611, May 2010.

[11] M. Pierobon and I. F. Akyildiz, "Capacity of a diffusion-based molecular communication system with channel memory and molecular noise," *IEEE Trans. Inf. Theory*, vol. 59, no. 2, pp. 942–954, Feb. 2013.

[12] K. V. Srinivas, A. W. Eckford, and R. S. Adve, "Molecular communication in fluid media: The additive inverse Gaussian noise channel," *IEEE Trans. Inf. Theory*, vol. 58, no. 7, pp. 4678–4692, July 2012.

[13] N. Farsad, A. W. Eckford, S. Hiyama, and Y. Moritani, "On-chip molecular communication: Analysis and design," *IEEE Trans. NanoBiosci.*, vol. 11, no. 3, pp. 304–314, Sept. 2012.

[14] S. Hiyama, Y. Moritani, R. Gojo, S. Takeuchi, and K. Sutoh, "Biomolecular-motor-based autonomous delivery of lipid vesicles as nano- or microscale reactors on a chip," *RSC Lab on a Chip*, vol. 10, no. 20, pp. 2741–2748, 2010.

[15] N. Farsad, A. W. Eckford, and S. Hiyama, "A Markov chain channel model for active transport molecular communication," *IEEE Trans. Signal Process.*, vol. 62, no. 9, pp. 2424–2436, May 2014.

[16] M. U. Mahfuz, D. Makrakis, and H. T. Mouftah, "On the characterization of binary concentration-encoded molecular communication in nanonetworks," *Elsevier Nano Commun. Netw.*, vol. 1, no. 4, pp. 289–300, Dec. 2010.

[17] L. C. Cobo and I. F. Akyildiz, "Bacteria-based communication in nanonetworks," *Elsevier Nano Commun. Netw.*, vol. 1, no. 4, pp. 244–256, Dec. 2010.

[18] H. B. Yilmaz, N.-R. Kim, and C.-B. Chae, "Effect of ISI mitigation on modulation techniques in molecular communication via diffusion," *Proc. ACM NanoCom*, vol. 3, 2014.

[19] N. Farsad, H. B. Yilmaz, A. W. Eckford, C.-B. Chae, and W. Guo, "A comprehensive survey of recent advancements in molecular communication," *IEEE Commun. Surveys Tuts.*, vol. 18, no. 3, pp. 1887 – 1919, thirdquarter 2016.

[20] N.-R. Kim and C.-B. Chae, "Novel modulation techniques using isomers as messenger molecules for nano communication networks via diffusion," *IEEE J. Sel. Areas Commun.*, vol. 31, no. 12, pp. 847–856, Dec. 2013.

[21] T. Nakano, Y. Okaie, and J.-Q. Liu, "Channel model and capacity analysis of molecular communication with brownian motion," *IEEE Commun. Lett.*, vol. 16, no. 6, pp. 797–800, June 2012.

[22] S. Ghavami, R. S. Adve, and F. Lahouti, "Information rates of ask-based molecular communication in fluid media," *IEEE Trans. Mol. Biol. Multi-Scale Commun.*, vol. 1, no. 3, pp. 277–291, Sept 2015.

[23] G. Aminian, H. Arjmandi, A. Gohari, M. Nasiri-Kenari, and U. Mitra, "Capacity of diffusion-based molecular communication networks over lti-poisson channels," *IEEE Trans. Mol. Biol. Multi-Scale Commun.*, vol. 1, no. 2, pp. 188–201, June 2015.

[24] B. Atakan, O. B. Akan, and S. Balasubramaniam, "Body area nanonetworks with molecular communications in nanomedicine," *IEEE Commun. Mag.*, vol. 50, no. 1, pp. 28–34, Jan. 2012.

[25] F. Dressler and S. Fischer, "Connecting in-body nano communication with body area networks: Challenges and opportunities of the internet of nano things," *Elsevier Nano Commun. Netw.*, vol. 6, no. 2, pp. 29 – 38, June 2015.

[26] N. Farsad, W. Guo, and A. W. Eckford, "Tabletop molecular communication: Text messages through chemical signals," *PLoS One*, vol. 8, no. 12, pp. e82935, Dec. 2013.

[27] B. H. Koo, C. Lee, H. B. Yilmaz, N. Farsad, A. Eckford, and C. B. Chae, "Molecular MIMO: From theory to prototype," *IEEE J. Sel. Areas Commun.*, vol. 34, no. 3, pp. 600–614, 2016.

[28] M. M. Rahman, A. J. S. Ahammad, J.-H. Jin, S. J. Ahn, and J.-J. Lee, "A comprehensive review of glucose biosensors based on nanostructured metal-oxides," *Sensors*, vol. 10, no. 5, pp. 4855–4886, May 2010.

[29] P. R. Solanki, A. Kaushik, V. V. Agrawal, and B. D. Malhotra, "Nanostructured metal oxide-based biosensors," *NPG Asia Mater.*, vol. 3, pp. 17–24, 2011.

[30] N. Farsad, N.-R. Kim, A. W. Eckford, and C.-B. Chae, "Channel and noise models for nonlinear molecular communication systems," *IEEE J. Sel. Areas Commun.*, vol. 32, no. 12, pp. 2392–2401, Dec. 2014.

[31] V. E. Bochenkov and G. B. Sergeev, "Sensitivity, selectivity, and stability of gas-sensitive metal-oxide nanostructures," *Metal Oxide Nanostruct. Their Appl.*, vol. 3, pp. 31–52, 2010.

[32] K.-W. Kim, P.-S. Cho, S.-J. Kim, J.-H Lee, C.-Y. Kang, J.-S. Kim, and S.-J. Yoon, "The selective detection of C_2H_5OH using SnO_2–ZnO thin film gas sensors prepared by combinatorial solution deposition," *Elsevier Sensor. Actuat. B-CHEM.*, vol. 123, no. 1, pp. 318–324, 2007.

[33] D. Kohl, "Surface processes in the detection of reducing gases with SnO2-based devices," *Elsevier Sensor. Actuat.*, vol. 18, no. 1, pp. 71–113, 1989.

[34] N. Yamazoe and K. Shimanoe, "Theory of power laws for semiconductor gas sensors," *Elsevier Sensor. Actuat. B-CHEM.*, vol. 128, no. 2, pp. 566–573, 2008.

[35] H. B. Yilmaz, A. C. Heren, T. Tugcu, and C.-B. Chae, "Three-dimensional channel characteristics for molecular communication with an absorbing receiver," *IEEE Commun. Lett.*, vol. 18, no. 6, pp. 929–932, June 2014.

[36] M. S. Kuran, H. B. Yilmaz, T. Tugcu, and I. F. Akyildiz, "Modulation techniques for communication via diffusion in nanonetworks," in *Proc. IEEE Int. Conf. on Commun. (ICC)*, 2011, pp. 1–5.

[37] N.-R. Kim and C.-B. Chae, "Novel modulation techniques using isomers as messenger molecules for molecular communication via diffusion," in *Proc. IEEE Int. Conf. on Commun. (ICC)*, 2012, pp. 6146–6150.

[38] N. Farsad, Y. Murin, W. Guo, C.-B. Chae, A. Eckford, and A. Goldsmith, "On the impact of time-synchronization in molecular timing channels," in *Proc. IEEE Glob. Commun. Conf. (GLOBECOM)*, 2016.

[39] H. B. Yilmaz and C.-B. Chae, "Simulation study of molecular communication systems with an absorbing receiver: Modulation and ISI mitigation techniques," *Elsevier Simul. Model. Pract. Theory*, vol. 49, pp. 136 – 150, Dec. 2014.

Na-Rae Kim (S'12 - M'16) received her B.S. and Ph.D degrees in chemical engineering and integrated technology from Yonsei University, Korea in 2011, and 2016. She is currently a postdoctoral research fellow with Singapore University of Technology and Design, working on molecular communication, internet of things, and body area networks. She is a recipient of National Research Fund Postdoctoral Fellowship of Korea, and the Best Demo Award at INFOCOM, 2015.

Nariman Farsad (S'07 - M'15) received his M.Sc. and Ph.D. degrees in computer science and engineering from York University, Toronto, ON, Canada in 2010 and 2015, respectively. He is currently a Postdoctoral Fellow with the Department of Electrical Engineering at Stanford University, where he is a recipient of Natural Sciences and Engineering Research Council of Canada (NSERC) Postdoctoral Fellowship. Nariman has won the second prize in 2014 IEEE ComSoc Student Competition: Communications Technology Changing the World, the best demo award at INFOCOM'15, and was recognized as a finalist for the 2014 Bell Labs Prize. Nariman has been an Area Associate Editor for IEEE Journal of Selected Areas of Communication–Special Issue on Emerging Technologies in Communications, and a Technical Reviewer for a number of journals including IEEE Transactions on Signal Processing, and IEEE Transactions on Communication. He was also a member of the Technical Program Committees for the ICC'2015, BICT'15, BICT'16, GLOBECOM'15, GLOBECOM'2016, GLOBECOM'2017.

Andrew W. Eckford (M'96 - S'99 - M'03 - SM'15) received the B.Eng. degree from the Royal Military College of Canada, Kingston, ON, Canada, in 1996, and the M.A.Sc. and Ph.D. degrees from the University of Toronto, Toronto, ON, Canada, in 1999 and 2004, respectively, all in electrical engineering. He is an Associate Professor with the Department of Electrical Engineering and Computer Science, York University, Toronto, ON. Canada. He held postdoctoral fellowships at the University of Notre Dame, Notre Dame, IN, USA, and the University of Toronto, prior to taking up a faculty position at York University in 2006. His research interests include the application of information theory to nonconventional channels and systems, especially the use of molecular and biological means to communicate. His research has been covered in media including *The Economist* and *The Wall Street Journal*. He is also a co-author of the textbook *Molecular Communication* (Cambridge University Press). He was a finalist for the 2014 Bell Labs Prize.

Chan-Byoung Chae (S'06 - M'09 - SM'12) is Underwood Distinguished Professor in the School of Integrated Technology, College of Engineering, Yonsei University, Korea. He was a member of technical staff at Bell Laboratories, Alcatel-Lucent, Murray Hill, NJ, USA. Before joining Bell Laboratories, he was with Harvard University, Cambridge, MA, USA as a post-doctoral fellow. He received the Ph.D. degree in Electrical and Computer Engineering from The University of Texas (UT), Austin, TX, USA in 2008, where he was a member of the Wireless Networking and Comm. Group (WNCG). Prior to joining UT, he was a research engineer at the Telecommunications R&D Center, Samsung Electronics, Korea, from 2001 to 2005. He serves/has served as an editor for the *IEEE Comm. Mag.* (2016-present), the *IEEE Trans. on Wireless Comm.* (2012-present), the *IEEE Trans. on Molecular, Biological, and Multi-scale Comm.* (2015-present), the *IEEE Wireless Comm. Letters* (2016-present), and the *IEEE/KICS Jour. Comm. Net.* (2012-present). He was a guest editor for the *IEEE Jour. Sel. Areas in Comm.* (2014-2015).

Dr. Chae was the recipient/co-recipient of of the Underwood Distinguished Professor Award from Yonsei University (2016), the Yonam Research Award from LG Yonam Foundation (2016), the Best Young Professor Award from the College of Engineering, Yonsei University (2015), the IEEE INFOCOM Best Demo Award (2015), the IEIE/IEEE Joint Award for Young IT Engineer of the Year (2014), the KICS Haedong Young Scholar Award (2013), the IEEE Sig. Proc. Mag. Best Paper Award (2013), the IEEE ComSoc AP Outstanding Young Researcher Award (2012), the IEEE VTS Dan. E. Noble Fellowship Award (2008) and two Gold Prizes (1st) in the 14th/19th Humantech Paper Contest. He also received the Korea Government Fellowship (KOSEF) during his Ph.D. studies.